Refractive Index Measurement by Gain- or Loss-Induced Resonance

Markus Miller

Using a semiconductor optical resonator consisting of a Bragg reflector and a total internal reflection mirror, a refractive index sensor can be realized. When absorption or gain is present within the resonator, sharp resonance peaks in the reflectivity spectrum can be observed. Since the phase of the reflected light at total internal reflection depends on the refractive indices at the interface, the resonance wavelength is related to the refractive indices. Analytical calculations and transfer matrix simulations are presented to explain the measurement principle in detail and show the potential of the new sensor approach.

1. Introduction

Refractive index sensors are widely used in industry, biology, and medicine for a variety of purposes like, for instance, the analysis of glucose concentration in honey, jam, or even blood. In order to achieve high-precision measurements and to reduce the size of the device compared to the traditional Abbe refractometer [1], new sensors based on surface plasmon resonance [2], optical fibers [3], or resonant optical tunneling [4] have been investigated and developed. Many of these approaches determine the refractive index from the spectral shift of a resonance that is related to the variation of the refractive index of the sample. Therefore, the spectral shift per refractive index unit as well as the spectral width of the resonance peak are important for precise measurements [5]. A high-quality resonator with high sensitivity to changes of refractive indices fulfills these requirements.

2. Measurement Principle

The measurement principle of the presented sensor is based on a resonator providing multiple beam interference to obtain sharp resonances and on total internal reflection producing an evanescent field for high sensitivity of the resonance wavelength to refractive index changes. A side-view of the structure is shown in Fig. 1. The device can be regarded as a half vertical-cavity surface-emitting laser obtained by cutting through the active zone in lateral direction. Thus the device consists of the substrate, the remaining distributed Bragg reflector (DBR), the active region with refractive index $\bar{n}_1$ and the sensing area at the bottom interface between the device and the adjacent medium of refractive index $\bar{n}_2$. For $\bar{n}_2 < \bar{n}_1$ and for angles Θ_1 larger than the critical angle $\Theta_c = \arcsin(\bar{n}_2/\bar{n}_1)$, total internal reflection occurs at the bottom interface. In this case only an evanescent field penetrates into the adjacent medium and the interface acts as an ideal mirror with

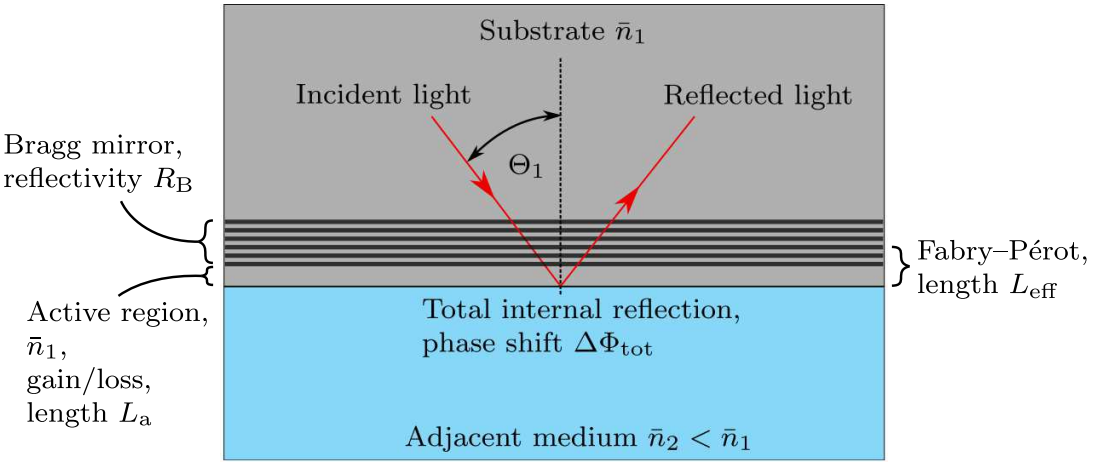

Fig. 1: Scheme of the measurement device consisting of substrate, DBR, active region, and the bottom interface to the adjacent medium.

a power reflectivity $R = P_\mathrm{r}/P_\mathrm{i} = 1$. The phase of the reflected light is shifted by $\Delta\Phi_\mathrm{tot}$. In the case of TE-polarized incident light, the phase shift $\Delta\Phi_\mathrm{tot,TE}$ is given by [6]

$$\Delta\Phi_\mathrm{tot,TE} = 2\arctan\frac{\sqrt{\bar{n}_1^2\sin^2\Theta_1 - \bar{n}_2^2}}{\bar{n}_1\cos\Theta_1} \tag{1}$$

and depends on the refractive indices $\bar{n}_1$ and $\bar{n}_2$ of the interface materials.

Total internal reflection and the DBR form a Fabry–Pérot cavity of effective length L_eff and a corresponding roundtrip phase Φ_FP in the TE-case of

$$\Phi_\mathrm{FP} = \frac{4\pi\bar{n}_\mathrm{eff}L_\mathrm{eff}\cos\Theta_1}{\lambda} - \Delta\Phi_\mathrm{tot,TE}, \tag{2}$$

where λ is the free-space wavelength and $\bar{n}_\mathrm{eff}$ is the effective refractive index of the resonator. When the roundtrip phase fulfills the condition $\Phi_\mathrm{FP} = m \cdot 2\pi$ with integer m, resonances occur at discrete wavelengths λ_m given by

$$\lambda_m = \frac{4\pi\bar{n}_\mathrm{res}L_\mathrm{eff}\cos\Theta_1}{m\cdot 2\pi + \Delta\Phi_\mathrm{tot,TE}}. \tag{3}$$

Thus, for a fixed angle of incidence, the resonance wavelength λ_m is a function of the refractive index of the adjacent medium, as the phase shift of total internal reflection $\Delta\Phi_\mathrm{tot,TE}$ depends on the refractive indices of both materials at the interface. Hence, for known device parameters, the refractive index of the adjacent medium can be obtained from the resonance wavelength.

Assuming a (positive or negative) absorption coefficient α in the active region of length L_a in an otherwise lossless device, the reflectivity as a function of the roundtrip phase Φ_FP is given by

$$R = \frac{(\sqrt{R_\mathrm{B}} - \exp(-\alpha L_\mathrm{a}))^2 + 4\sqrt{R_\mathrm{B}}\exp(-\alpha L_\mathrm{a})\sin^2(\Phi_\mathrm{FP}/2)}{(1-\sqrt{R_\mathrm{B}}\exp(-\alpha L_\mathrm{a}))^2 + 4\sqrt{R_\mathrm{B}}\exp(-\alpha L_\mathrm{a})\sin^2(\Phi_\mathrm{FP}/2)}, \tag{4}$$

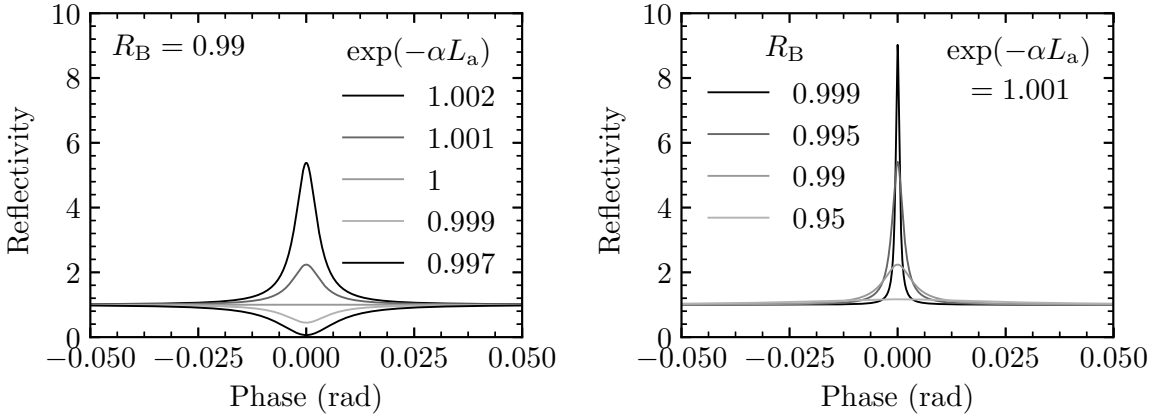

Fig. 2: Reflectivity R according to (4) plotted over the roundtrip phase for different absorption $\exp(-\alpha L_a)$ with fixed reflectivity R_B (left) and different Bragg reflectivities R_B with fixed amplification $\exp(-\alpha L_a) = 1.001$ (right).

where R_B is the reflectivity of the DBR and the reflectivity of the total internal reflection mirror is set to one. Equation (4) is plotted in Fig. 2 as function of the roundtrip phase. On the left-hand side the reflectivity is shown for different absorption and amplification $\exp(-\alpha L_a)$ in the active region and a fixed Bragg reflectivity, whereas on the right-hand side the reflectivity is displayed for a fixed amplification but varying DBR reflectivities R_B. For a phase equal to zero or $m \cdot 2\pi$, a clear dip or peak can be observed in Fig. 2, depending on the sign of the absorption coefficient. In the lossless case, no resonance occurs because of the ideal total internal reflection mirror. The height and half-width of the resonance depend on the DBR reflectivity as well as the absorption or gain. With increasing Bragg reflectivity the half-width of the resonance peak shrinks, as known for increasing finesse of a Fabry–Pérot resonator. Especially when gain is present within the active zone, the peak height and half-width depend strongly on the mirror reflectivity, resulting in a narrow, high peak for high DBR reflectivity.

3. Transfer Matrix Simulations

The transfer matrix method is a proper one-dimensional simulation approach to investigate the behavior of layered media devices, as it is possible to calculate reflectivity spectra as well as field distributions within the structure [7]. Therefore this method is used to design and analyze the structure of the presented sensor device based on III–V semiconductor materials. III–V compounds offer the possibility to incorporate quantum wells in the structure as absorbing or amplifying layers. All simulations presented in the following assume TE-polarized incident light.

Figure 3 shows the refractive index profile of the designed layer structure on the left-hand side and corresponding reflectivity spectra for normal incidence on the right side. The layer structure consists of a GaAs substrate on top, followed by 15 Bragg mirror pairs with GaAs of assumed refractive index equal to 3.6 as high-index layer and AlAs of refractive index equal to 3 as low-index layer. A 10 nm InGaAs quantum well of

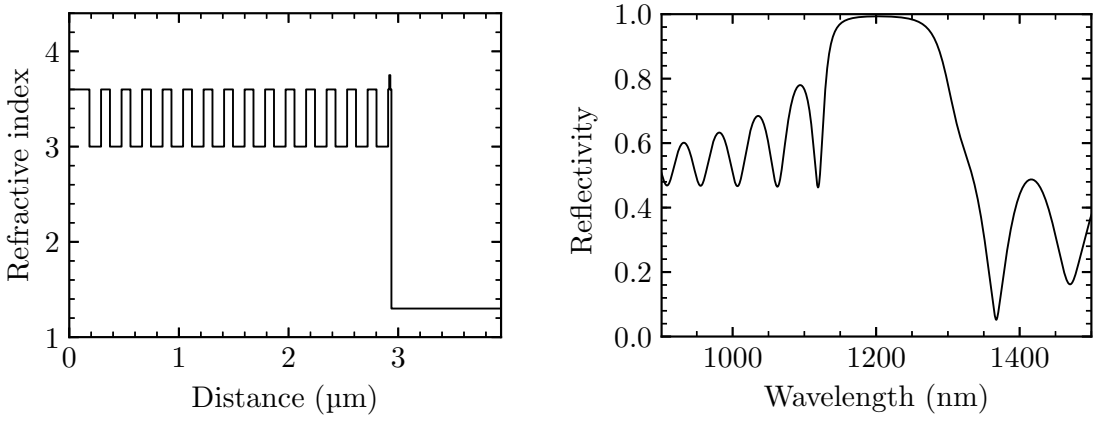

Fig. 3: Semiconductor layer sequence of the device containing 15 Bragg mirror pairs and a single quantum well (left) with corresponding reflectivity spectrum for normal incidence (right).

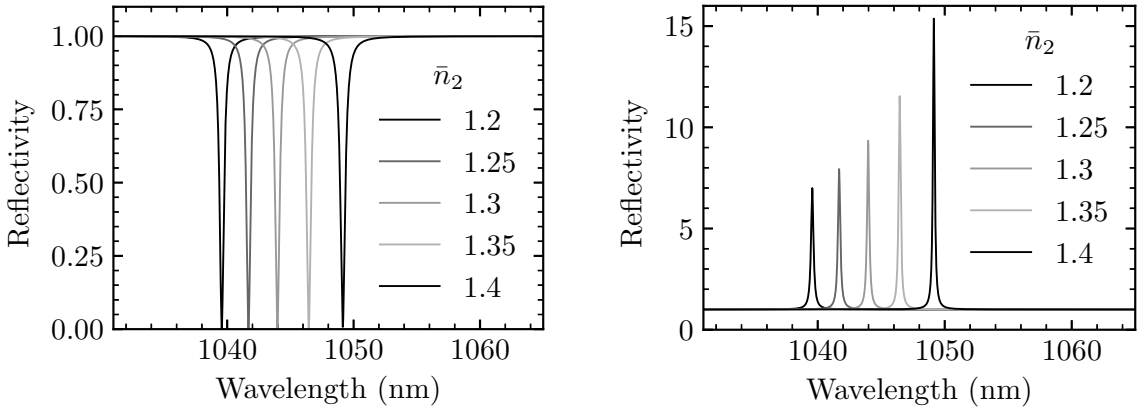

Fig. 4: Calculated reflectivity spectra at fixed angle of incidence ($\Theta_1 = 30.5\,^\circ$) for different refractive indices of the sample with absorption (left) or gain (right) in the quantum well.

refractive index 3.75 incorporated in thin GaAs layers is placed between the DBR and the interface to the adjacent medium of refractive index $\bar{n}_2$. Dispersion is neglected in all simulations and absorption only occurs within the quantum well, as described by the intensity absorption coefficient α. The Bragg mirror in Fig. 3 is designed to achieve high reflectivity at wavelengths of 1040 nm for an angle of incidence of about $30.5\,^\circ$ to obtain total internal reflection at the bottom interface. Thus the reflectivity spectrum for normal incidence in Fig. 3 is shifted towards longer wavelengths of about 1200 nm and its maximum reflectivity is lower compared to the angled incidence case.

In Fig. 4 calculated reflectivity spectra of the designed structure for an angle of incidence of $\Theta_1 = 30.5\,^\circ$ and various refractive indices of the sample are shown for an absorption coefficient of $\alpha = 500\,\mathrm{cm}^{-1}$ on the left and a gain coefficient of $\alpha = -1000\,\mathrm{cm}^{-1}$ on the right. In both cases a red-shift of the resonance wavelength with increasing refractive indices $\bar{n}_2$ can be observed, as the phase shift due to total internal reflection decreases towards zero with increasing refractive index of the adjacent medium. The shift rate is

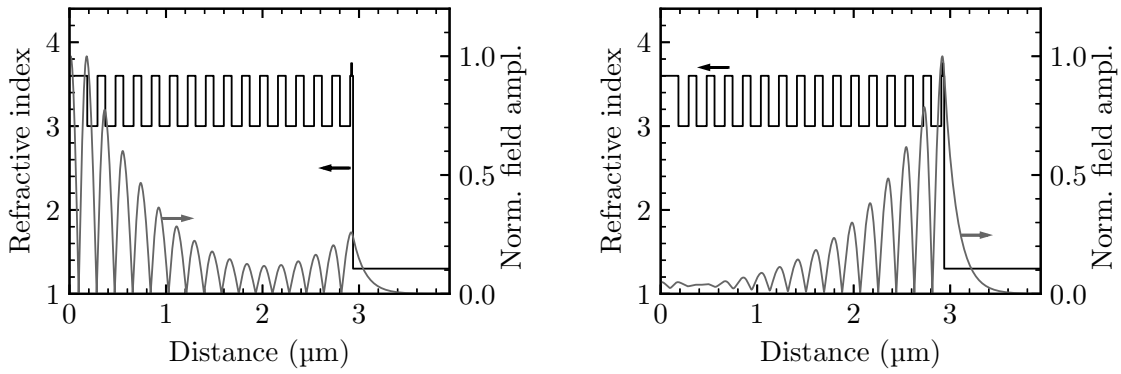

Fig. 5: Field distributions along the device for a sample with refractive index $\bar{n}_2 = 1.3$, a quantum well absorption coefficient $\alpha = -1000\,\mathrm{cm}^{-1}$, and an angle of incidence $\Theta_1 = 30.5\,^\circ$ for wavelengths $\lambda = 1030\,\mathrm{nm}$ (left) and $\lambda = 1044\,\mathrm{nm}$ (right).

$\Delta\lambda/\Delta\bar{n}_2 \approx 50\,\mathrm{nm}$. The depth or height of the resonance differs as the reflectivity of the DBR is wavelength-dependent. This effect is especially seen when gain is present within the quantum well.

Figure 5 shows the field distributions for an adjacent medium of refractive index $\bar{n}_2 = 1.3$ and a quantum well absorption coefficient $\alpha = -1000\,\mathrm{cm}^{-1}$ for a non-resonant case at $\lambda = 1030\,\mathrm{nm}$ on the left and resonant behavior at $\lambda = 1044\,\mathrm{nm}$ on the right. At the interface to the adjacent medium, the evanescent field with a penetration depth of less than 500 nm is observable in both plots. In the non-resonant case, the field amplitude is small at the interface and the quantum well position compared to the incident amplitude. In contrast, in the resonant case, the field amplitude is over 20 times larger at the quantum well compared to the incident amplitude. Thus, the interaction with the quantum well is strong in the resonant case, leading to high absorption or amplification, depending on the excitation level of the quantum well. The small penetration depth of the evanescent field makes the sensor sensitive to refractive index changes of thin layers.

4. Conclusion

The presented refractive index measurement principle shows high potential as it is capable of measuring refractive indices over a wide range with high accuracy. The device structure is fairly simple and can be fabricated with common semiconductor epitaxial growth technologies. Of course, in a next step, the theoretical potential must be validated in experiments. Therefore, the coupling of the incident light into the semiconductor substrate to achieve total internal reflection at the bottom interface has to be considered. As the index contrast between air and GaAs is high, no direct light coupling into a planar GaAs slab to achieve the necessary angle above the critical angle in the semiconductor device is possible. In order to achieve sufficiently large angles of incidence at the interface, input light coupling via prisms or diffraction gratings can provide a solution.

References

[1] W. Boyes (Ed.), *Instrumentation Reference Book* (4th ed.), Burlington, MA, USA: Butterworth-Heinemann, 2010.

[2] J. Zeng and D. Liang, "Application of fiber optic surface plasmon resonance sensor for measuring liquid refractive index", *J. Intell. Material Syst. Struct.*, vol. 17, pp. 787–791, 2006.

[3] M. Naora, S. Taue, and H. Fukano, "Ultrasensitive fiber-optic refractive index sensor based on multimode interference with fiber-loop technique", in Proc. *22nd Microoptics Conference (MOC)*, pp. 130–131. Tokyo, Japan, Nov. 2017.

[4] A.Q. Jian, X.M. Zhang, W.M. Zhu, and M. Yu, "Optofluidic refractometer using resonant optical tunneling effect", *Biomicrofluidics*, vol. 4, pp. 043008-1–11, 2010.

[5] I.M. White and X. Fan, "On the performance quantification of resonant refractive index sensors", *Optics Express*, vol. 16, pp. 1020–1028, 2008.

[6] K.J. Ebeling, *Integrated Optoelectronics*, Berlin: Springer-Verlag, 1993.

[7] P. Yeh, *Optical Waves in Layered Media*, New York: John Wiley & Sons, 1988.